

# Optimum Biped Trajectory Planning for Humanoid Robot Navigation in Unseen Environment

Hanafiah Yussof<sup>1,2</sup> and Masahiro Ohka<sup>1</sup>

<sup>1</sup>*Graduate School of Information Science, Nagoya University  
Japan*

<sup>2</sup>*Faculty of Mechanical Engineering, Universiti Teknologi MARA  
Malaysia*

## 1. Introduction

The study on biped locomotion in humanoid robots has gained great interest since the last decades (Hirai et. al. 1998, Hirukawa et. al., 2004, Ishiguro, 2007). This interest are motivated from the high level of mobility, and the high number of degrees of freedom allow this kind of mobile robot adapt and move upon very unstructured sloped terrain. Eventually, it is more desirable to have robots of human build instead of modifying environment for robots (Khatib et. al, 1999). Therefore, a suitable navigation system is necessary to guide the robot's locomotion during real-time operation. In fundamental robot navigation studies, robot system is normally provided with a map or a specific geometrical guidance to complete its tasks (Okada et al., 2003, Liu et al., 2002). However during operation in uncertain environment such as in emergency sites like an earthquake site, or even in a room that the robots never been there before, which is eventually become the first experience for them, robots needs some intelligence to recognize and estimate the position and structure of objects around them. The most important is robot must localize its position within this environment and decide suitable action based on the environment conditions. To archives its target tasks, the robot required a highly reliable sensory devices for vision, scanning, and touching to recognize surrounding. These problems have become the main concern in our research that deals with humanoid robot for application in built-for-human environment.

Operation in unseen environment or areas where visual information is very limited is a new challenge in robot navigation. So far there was no much achievement to solve robot navigation in such environments. In previous research, we have proposed a contact interaction-based navigation strategy in a biped humanoid robot to operate in unseen environment (Hanafiah et al., 2008). In this chapter, we present analysis results of optimum biped trajectory planning for humanoid robot navigation to minimize possibility of collision during operation in unseen environment. In this analysis, we utilized 21-dof biped humanoid robot Bonten-Maru II. Our aim is to develop reliable walking locomotion in order

to support the main tasks in the humanoid robot navigation system. Fig. 1 shows diagram of humanoid robot Bonten-Maru II and its configurations of dofs.

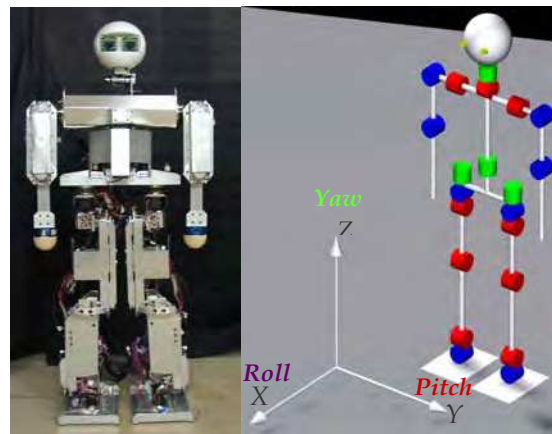


Fig. 1. Humanoid Robot Bonten-Maru II and its configuration of dofs.

It is inevitable that stable walking gait strategy is required to provide efficient and reliable locomotion for biped robots. In the biped locomotion towards application in unseen environment, we identified three basic motions: walk forward and backward directions, side-step to left and right, and yawing movement to change robot's orientation. In this chapter, at first we analyzed the joint trajectory generation in humanoid robot legs to define efficient gait pattern. We present kinematical solutions and optimum gait trajectory patterns for humanoid robot legs. Next, we performed analysis to define efficient walking gait locomotion by improvement of walking speed and travel distance without reducing reduction-ratio at joint-motor system. This is because sufficient reduction-ratio is required by the motor systems to supply high torque to the robot's manipulator during performing tasks such as object manipulation and obstacle avoidance. We also present optimum yawing motion strategy for humanoid robot to change its orientation within confined space. The analysis results were verified with simulation and real-time experiment with humanoid robot Bonten-Maru II.

Eventually, to safely and effectively navigate robots in unseen environment, the navigation system must feature reliable collision checking method to avoid collisions. In this chapter, we present analyses of collision checking using the robot arms to perform searching, touching and grasping motions in order to recognize its surrounding condition. The collision checking is performed in searching motion of the robot's arms that created a radius of detection area within the arm's reach. Based on the searching area coverage of the robot arms, we geometrically analyze the robot biped motions using Rapid-2D CAD software to identify the ideal collision free area. The collision free area is used to calculate maximum biped step-length when no object is detected. Consequently the robot control system created an absolute collision free area for the robot to generate optimum biped trajectories. In case of object is detected during searching motion, the robot arm will touch and grasp the object surface to define self-localization, and consequently optimum step-length is refined.

Verification experiments were conducted using humanoid robot Bonten-Maru II to operate in a room with walls and obstacles was conducted. In this experiment, the robot visual sensors are not connected to the system. Therefore the robot locomotion can only rely on contact interaction of the arms that are equipped with force sensors.

## 2. Short Survey on Humanoid Robot Navigation

Operation in unseen environment or areas where visual information is very limited is a new challenge in robot navigation. So far there was no much achievement to solve robot navigation in such environments. In normal conditions, it is obvious that a navigation system that applies non-contact sensors such as vision sensors provides intensive information about the environment (Sagues & Guerrero, 1999). However, robots cannot just rely on this type of sensing information to effectively work and cooperate with humans. For instance, in real applications the robots are likely to be required to operate in areas where vision information is very limited, such as in a dark room or during a rescue mission at an earthquake site (Diaz et. al., 2001). Moreover vision sensors have significant measurement accuracy problems resulting from technical problems such as low camera resolution and the dependence of stereo algorithms on specific image characteristics. Furthermore, the cameras are normally located at considerable distance from objects in the environment where operation takes place, resulting in approximate information of the environment.

In addition to the above, a laser range finder has also been applied in a robot navigation system (Thompson et. al., 2006). This sensor is capable of producing precise distance information and provides more accurate measurements compared with the vision sensor. However, it is impractical to embed this type of sensor with its vision analysis system in a walking robot system because of its size and weight (Okada et. al., 2003). A navigation system that applies contact-based sensors is capable of solving the above problems, particularly for a biped walking robot system (Hanafiah et. al., 2007). This type of sensor can accurately gauge the structure of the environment, thus making it suitable to support current navigation systems that utilize non-contact sensors. Furthermore, the system architecture is simpler and can easily be mounted on the walking robot body.

Eventually, to safely and effectively navigate robots in unseen environment, the navigation system must feature reliable collision checking method to avoid collisions. To date, in collision checking and prediction research, several methods such as vision based local floor map (Okada et al., 2003, Liu et al., 2002) and cylinder model (Guttmann et al., 2005) have been proposed for efficient collision checking and obstacle recognition in biped walking robot. In addition, Kuffner (Kuffner et al., 2002) have used fast distance determination method for self-collision detection and prevention for humanoid robots. This method is for convex polyhedra in order to conservatively guarantee that the given trajectory is free of self-collision. However, to effectively detect objects based on contact-based sensors, such methods are not suitable because they are mostly based on assumption of environment conditions acquired by non-contact sensors such as vision and laser range sensors.

Several achievements have been reported related with navigation in humanoid robots. Ogata have proposed human-robot collaboration based on quasi-symbolic expressions applying humanoid on static platform named Robovie (Ogata et al., 2005). This work combined non-contact and contact sensing approach in collaboration of human and robot during navigation tasks. This is the closest work with the approach used in this research.

However Ogata use humanoid robot without leg. On the other hand, related with biped humanoid robot navigation, the most interesting work was presented by Stasse where visual 3D Simultaneous Localization and Mapping (SLAM) was used to navigate HRP-2 humanoid robot performing visual loop-closing motion (Stasse et al., 2006). In other achievements, Gutmann (Gutmann et al., 2005) have proposed real-time path planning for humanoid robot navigation. The work was evaluated using QRIO Sony's small humanoid robot equipped with stereo camera. Meanwhile, Seara have evaluated methodological aspects of a scheme for visually guided humanoid robot navigation using simulation (Seara et al., 2004). Next, Okada have proposed humanoid robot navigation system using vision based local floor map (Okada et al., 2003). Related with sensory-based biped walking, Ogura (Ogura et al., 2004) has proposed a sensory-based biped walking motion instruction strategy for humanoid robot using visual and auditory sensors to generate walking patterns according to human orders and to memorize various complete walking patterns. In previous research, we have proposed a contact interaction-based navigation strategy in a biped humanoid robot to operate in unseen environment (Hanafiah et. al., 2008). In this chapter, we present analysis results of optimum biped trajectory planning for humanoid robot navigation to minimize possibility of collision during operation in unseen environment.

### 3. Simplification of Kinematics Solutions

A reliable trajectory generation formulations will directly influence stabilization of robot motion especially during operation in unseen environment where the possibility of unstable biped walking due to ground condition and collision with unidentified objects are rather high if compared to operation in normal condition. In this chapter, at first we analyzed the joint trajectory generation in humanoid robot legs to define efficient gait pattern. We present kinematical solutions and optimum gait trajectory patterns for humanoid robot legs.

Eventually, formulations to generate optimum trajectory in articulated joints and manipulators are inevitable in any types of robots, especially for legged robot. Indeed, the most sophisticated forms of legged motion are that of biped gait locomotion. However calculation to solve kinematics problems to generate trajectory for robotic joints is a complicated and time-consuming study, especially when it involves a complex joint structure. Furthermore, computation of joint variables is also needed to compute the required joint torques for the actuators. In current research, to generate optimum robot trajectory, we simplified kinematics formulation to generate trajectory for each robot joint in order to reduce calculation time and increase reliability of robot arms and legs motions. This is necessary because during operation in unseen environment, robot will mainly rely on contact interaction using its arms. Consequently, an accurate and fast respond of robot's both legs are very important to maintain stability of its locomotion.

We implemented a simplified approach to solving inverse kinematics problems by classifying the robot's joints into several groups of joint coordinate frames at the robot's manipulator. To describe translation and rotational relationship between adjacent joint links, we employ a matrix method proposed by Denavit-Hartenberg (Denavit & Hartenberg, 1955), which systematically establishes a coordinate system for each link of an articulated chain. Since this chapter focusing on biped trajectory, we present kinematical analysis of 6-dofs leg in the humanoid robot Bonten-Maru II body.

### 3.1 Kinematical Solutions of 6-DOFs Leg

Each of the legs has six dofs: three dofs (yaw, roll and pitch) at the hip joint, one dof (pitch) at the knee joint and two dofs (pitch and roll) at the ankle joint. In this research, we solve only inverse kinematics calculations for the robot leg. Figure 2 shows the structure and configuration of joints and links in the robot's leg. A reference coordinate is taken at the intersection point of the 3-dofs hip joint.

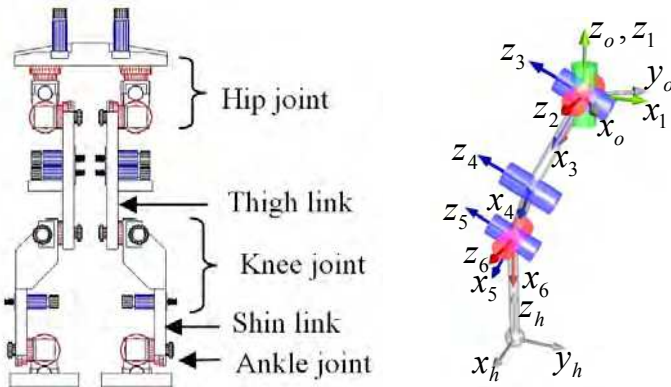


Fig. 2. Leg structure of Bonten-Maru II and configurations of joint coordinates.

Link	$\theta_{i\text{leg}}$	$d$	$\alpha$	$l$
0	$\theta_{1\text{leg}} + 90^\circ$	0	0	0
1	$\theta_{2\text{leg}} - 90^\circ$	0	$90^\circ$	0
2	$\theta_{3\text{leg}}$	0	$90^\circ$	0
3	$\theta_{4\text{leg}}$	0	0	$l_1$
4	$\theta_{5\text{leg}}$	0	0	$l_2$
5	$\theta_{6\text{leg}}$	0	$-90^\circ$	0
6	0	0	0	$l_3$

Table 1. Link parameters of the 6-dofs humanoid robot leg.

In solving calculations of inverse kinematics for the leg, the joint coordinates are divided into eight separate coordinate frames as listed below:

$\Sigma_0$  : Reference coordinate.

$\Sigma_1$  : Hip yaw coordinate.

$\Sigma_2$  : Hip roll coordinate.

$\Sigma_3$  : Hip pitch coordinate.

$\Sigma_4$  : Knee pitch coordinate.

$\Sigma_5$  : Ankle pitch coordinate.

$\Sigma_6$  : Ankle roll coordinate.

$\Sigma_h$  : Foot bottom-center coordinate.

Figure 2 also shows a model of the robot leg that indicates the configurations and orientation of each set of joint coordinates. Here, link length for the thigh is  $l_1$ , while for the shin it is  $l_2$ . Link parameters for the leg are defined in Table 1. From the Denavit-Hartenberg convention mentioned above, definitions of the homogeneous transform matrix of the link parameters can be described as follows:

$${}^0_h \mathbf{T} = \text{Rot}(z_i, \theta_i) \text{Trans}(0, 0, d_i) \text{Trans}(l_i, 0, 0) \text{Rot}(x_i, \alpha_i). \quad (1)$$

Here, variable factor  $\theta_i$  is the joint angle between the  $x_{i-1}$  and the  $x_i$ -axes measured about the  $z_i$  axis;  $d_i$  is the distance from the  $x_{i-1}$  axis to the  $x_i$  axis measured along the  $z_i$  axis;  $\alpha_i$  is the angle between the  $z_i$  axis to the  $z_{i-1}$  axis measured about the  $x_{i-1}$  axis, and  $l_i$  is the distance from the  $z_i$  axis to the  $z_{i-1}$  axis measured along the  $x_{i-1}$  axis. Referring to Fig. 2, the transformation matrix at the bottom of the foot ( ${}^6_h \mathbf{T}$ ) is an independent link parameter because the coordinate direction is changeable. Here, to simplify the calculations, the ankle joint is positioned so that the bottom of the foot settles on the floor surface. The leg's orientation is fixed from the reference coordinate so that the third row of the rotation matrix at the leg's end becomes like equation (2).

$$P_{zleg} = [0 \ 0 \ I]^T \quad (2)$$

Furthermore, the leg's links are classified into three groups to short-cut the calculations, where each group of links is calculated separately as follows:

- i) From link 0 to link 1 (Reference coordinate to coordinate joint number 1).
- ii) From link 1 to link 4 (Coordinate joint no. 2 to coordinate joint no. 4).
- iii) From link 4 to link 6 (Coordinate joint no. 5 to coordinate at the bottom of the foot).

Basically, i) is to control leg rotation at the  $z$ -axis, ii) is to define the leg position, while iii) is to decide the leg's end-point orientation. A coordinate transformation matrix can be arranged as following.

$${}^0_h \mathbf{T} = {}^0_1 \mathbf{T} {}^1_4 \mathbf{T} {}^4_h \mathbf{T} = ({}^0_h \mathbf{T}) ({}^1_2 \mathbf{T} {}^2_3 \mathbf{T} {}^3_4 \mathbf{T}) ({}^4_5 \mathbf{T} {}^5_6 \mathbf{T} {}^6_h \mathbf{T}) \quad (3)$$

Here, the coordinate transformation matrices for  ${}^1_4 \mathbf{T}$  and  ${}^4_h \mathbf{T}$  can be defined as (4) and (5), respectively.

$${}^1_4 \mathbf{T} = {}^1_2 \mathbf{T} {}^2_3 \mathbf{T} {}^3_4 \mathbf{T}$$

$$= \begin{bmatrix} s_2 c_{34} & -s_2 s_{34} & -c_2 & l_1 s_2 c_3 \\ -s_{34} & -c_{34} & 0 & -l_1 s_3 \\ -c_2 c_{34} & c_2 s_{34} & -s_2 & -l_1 c_2 c_3 \\ 0 & 0 & 0 & 1 \end{bmatrix} \quad (4)$$

$${}^4_h \mathbf{T} = {}^4_5 \mathbf{T} {}^5_6 \mathbf{T} {}^6_h \mathbf{T}$$

$$= \begin{bmatrix} c_5 c_6 & -c_5 s_6 & -s_5 & l_2 + l_3 c_5 c_6 \\ s_5 c_6 & -s_5 s_6 & c_5 & l_3 s_5 c_6 \\ -s_6 & -c_6 & 0 & -l_3 s_6 \\ 0 & 0 & 0 & 1 \end{bmatrix} \quad (5)$$

The coordinate transformation matrix for  ${}^0_h \mathbf{T}$ , which describes the leg's end-point position and orientation, can be shown with the following equation.

$${}^0_h \mathbf{T} = \begin{bmatrix} r_{11} & r_{12} & r_{13} & p_x \\ r_{21} & r_{22} & r_{23} & p_y \\ r_{31} & r_{32} & r_{33} & p_z \\ 0 & 0 & 0 & 1 \end{bmatrix} \quad (6)$$

From equation (2), the following conditions were satisfied.

$$r_{13} = r_{23} = r_{31} = r_{32} = 0, \quad r_{33} = 1 \quad (7)$$

Hence, joint rotation angles  $\theta_{1\text{leg}} \sim \theta_{6\text{leg}}$  can be defined by applying the above conditions. First, considering i), in order to provide rotation at the z-axis, only the hip joint needs to rotate in the yaw direction, specifically by defining  $\theta_{1\text{leg}}$ . As mentioned earlier, the bottom of the foot settles on the floor surface; therefore, the rotation matrix for the leg's end-point measured from the reference coordinate can be defined by the following equation.

$${}^0_h \mathbf{R} = \text{Rot}(z, \theta_{1\text{leg}})$$

$$= \begin{bmatrix} c\theta_{1\text{leg}} & -s\theta_{1\text{leg}} & 0 \\ s\theta_{1\text{leg}} & c\theta_{1\text{leg}} & 0 \\ 0 & 0 & 1 \end{bmatrix} = \begin{bmatrix} r_{11} & r_{12} & 0 \\ r_{21} & r_{22} & 0 \\ 0 & 0 & 1 \end{bmatrix} \quad (8)$$

Here,  $\theta_{1\text{leg}}$  can be defined as below.

$$\theta_{1\text{leg}} = \text{atan2}(r_{21}, r_{22}) \quad (9)$$

Next, considering ii), from the obtained result of  $\theta_{1\text{leg}}$ ,  ${}^0_h \mathbf{T}$  is defined in (9).

$${}^0_h \mathbf{T} = \begin{bmatrix} -s_I & -c_I & 0 & P_{x\text{leg}} \\ c_I & -s_I & 0 & P_{y\text{leg}} \\ 0 & 0 & 1 & P_{z\text{leg}} \\ 0 & 0 & 0 & 1 \end{bmatrix} \quad (10)$$

Here, from constrain orientation of the leg's end point, the position vector of joint 5 is defined as follows in (11), and its relative connection with the matrix is defined in (12). Next, equation (13) is defined relatively.

$${}^0 \mathbf{P}_5 = {}^0_4 \mathbf{T}^4 \mathbf{P}_5 = \begin{bmatrix} P_{x\text{leg}} & P_{y\text{leg}} & P_{z\text{leg}} & -l_3 \end{bmatrix}^T, \quad (11)$$

$${}^I_4 T^4 \hat{\mathbf{P}}_5 = {}^I_4 T^{-1} {}^0 \mathbf{P}_5 \quad (12)$$

$$\begin{bmatrix} s_2 c_{34} & -s_2 s_{34} & -c_2 & l_1 s_2 c_3 \\ -s_{34} & -c_{34} & 0 & -l_1 s_3 \\ -c_2 c_{34} & c_2 s_{34} & -s_2 & -l_1 c_2 c_3 \\ 0 & 0 & 0 & 1 \end{bmatrix} \begin{bmatrix} l_2 \\ 0 \\ 0 \\ 1 \end{bmatrix} = \begin{bmatrix} -s_I & c_I & 0 & 0 \\ -c_I & -s_I & 0 & 0 \\ 0 & 0 & 1 & 0 \\ 0 & 0 & 0 & 1 \end{bmatrix} \begin{bmatrix} p_x \\ p_y \\ p_z \\ -l_3 \end{bmatrix} \quad (13)$$

Therefore,

$$\begin{bmatrix} \hat{P}_{x\text{leg}} \\ \hat{P}_{y\text{leg}} \\ \hat{P}_{z\text{leg}} \end{bmatrix} = \begin{bmatrix} s_2(l_1 c_3 + l_2 c_{34}) \\ -(l_1 c_3 + l_2 s_{34}) \\ -c_2(l_1 c_3 + l_2 c_{34}) \end{bmatrix}. \quad (14)$$

To define joint angles  $\theta_{2\text{leg}}$ ,  $\theta_{3\text{leg}}$ ,  $\theta_{4\text{leg}}$ , equation (14) is used. Therefore, the rotation angles are defined as the following equations:

$$\theta_{4\text{leg}} = \text{atan}2\left(\pm\sqrt{1-C^2}, C\right) \quad (15)$$

$$\theta_{3\text{leg}} = \text{atan}2\left(\hat{p}_{xz\text{leg}}, \hat{p}_{y\text{leg}}\right) + \text{atan}2(k_1, k_2) \quad (16)$$

$$\theta_{2\text{leg}} = \text{atan}2\left(\hat{p}_{x\text{leg}}, \hat{p}_{z\text{leg}}\right). \quad (17)$$

Eventually,  $C$ ,  $\hat{p}_{xz\text{leg}}$ ,  $k_1$ ,  $k_2$  are defined as follows:

$$C = \frac{\hat{p}_{x\text{leg}}^2 + \hat{p}_{y\text{leg}}^2 + \hat{p}_{z\text{leg}}^2 - (l_1^2 + l_2^2)}{2l_1l_2} \quad (18)$$

$$\hat{p}_{xz\text{leg}} = \sqrt{\hat{p}_{x\text{leg}}^2 + \hat{p}_{z\text{leg}}^2} \quad (19)$$

$$k_1 = l_1 + l_2 c_4, \quad k_2 = -l_2 s_4 \quad (20)$$

Finally, considering iii), joint angles  $\theta_{5\text{leg}}$  and  $\theta_{6\text{leg}}$  are defined geometrically by the following equations:

$$\theta_{5\text{leg}} = -\theta_{3\text{leg}} - \theta_{4\text{leg}} \quad (21)$$

$$\theta_{6\text{leg}} = -\theta_{2\text{leg}}. \quad (22)$$

### 3.2 Interpolation and Gait Trajectory Pattern

A common way of making a robot's manipulator to move from start point to end point in a smooth, controlled fashion is to have each joint to move as specified by a smooth function of time  $t$ . Each joint starts and ends its motion at the same time, thus the robot's motion appears to be coordinated. In this research, we employ degree-5 polynomial equations to solve interpolation from start point  $P_0$  to end point  $P_f$ . Degree-5 polynomial equations provides smoother gait trajectory compared to degree-3 polynomial equations which commonly used in robotic control. Velocity and acceleration at  $P_0$  and  $P_f$  are defined as zero; only the position factor is considered as a coefficient for performing interpolation.

$$P(t) = a_0 + a_1 t + a_2 t^2 + a_3 t^3 + a_4 t^4 + a_5 t^5 \quad (23)$$

Time factor at  $P_0$  and  $P_f$  are describe as  $t_0 = 0$  and  $t_f$ , respectively. Here, boundary condition for each position, velocity and acceleration at  $P_0$  and  $P_f$  are shown at following equations.

$$\left. \begin{array}{l} P(0) = a_0 = P_o \\ \dot{P}(0) = a_1 = \dot{P}_o \\ \ddot{P}(0) = 2a_2 = \ddot{P}_o \\ P(t_f) = a_0 + a_1 t_f + a_2 t_f^2 + a_3 t_f^3 + a_4 t_f^4 + a_5 t_f^5 = P_f \\ \dot{P}(t_f) = a_1 + 2a_2 t_f + 3a_3 t_f^2 + 4a_4 t_f^3 + 5a_5 t_f^4 = \dot{P}_f \\ \ddot{P}(t_f) = 2a_2 + 6a_3 t_f + 12a_4 t_f^2 + 20a_5 t_f^3 = \ddot{P}_f \end{array} \right\} \quad (24)$$

Here, coefficient  $a_i$  ( $i = 0,1,2,3,4,5$ ) are defined by solving deviations of above equations. Results of the deviations are shown at below equations.

$$\left. \begin{array}{l} a_0 = y_o \\ a_1 = \dot{y}_o \\ a_2 = \frac{1}{2} \ddot{y}_o \\ a_3 = \frac{1}{2t_f^3} \{20(y_f - y_o) - (8\dot{y}_f + 12\dot{y}_o)t_f + (\ddot{y}_f - 3\ddot{y}_o)t_f^2\} \\ a_4 = \frac{1}{2t_f^4} \{-30(y_f - y_o) + (14\dot{y}_f + 16\dot{y}_o)t_f - (2\ddot{y}_f - 3\ddot{y}_o)t_f^2\} \\ a_5 = \frac{1}{2t_f^5} \{12(y_f - y_o) - 6(\dot{y}_f + \dot{y}_o)t_f + (\ddot{y}_f - \ddot{y}_o)t_f^2\} \end{array} \right\} \quad (25)$$

As mentioned before, velocity and acceleration at  $P_0$  and  $P_f$  were considered as zero, as shown in (26).

$$\dot{P}(0) = \ddot{P}(0) = \dot{P}(t_f) = \ddot{P}(t_f) = 0. \quad (26)$$

Generation of motion trajectories from points  $P_0$  to  $P_f$  only considered the position factor. Therefore, by given only positions data at  $P_0$  and  $P_f$ , respectively described as  $y_o$  and  $y_f$ , coefficients  $a_i$  ( $i = 0,1,2,3,4,5$ ) were solved as below.

$$\left. \begin{array}{l} a_0 = y_o \\ a_1 = 0 \\ a_2 = 0 \\ a_3 = \frac{10}{t_f^3} (y_f - y_o) \\ a_4 = -\frac{15}{t_f^4} (y_f - y_o) \\ a_5 = \frac{6}{t_f^5} (y_f - y_o) \end{array} \right\} \quad (27)$$

Finally, degree-5 polynomial function is defined as following equation.

$$y(t) = y_o + 10(y_f - y_o)u^3 - 15(y_f - y_o)u^4 + 6(y_f - y_o)u^5 \quad (28)$$

Where,

$$u = \frac{t}{t_f} = \frac{\text{current time}}{\text{motion time}}. \quad (29)$$

These formulations provide smooth and controlled motion trajectory to the robot's manipulators during performing tasks in the proposed navigation system. Consequently, to perform a smooth and reliable gait, it is necessary to define step-length and foot-height during transferring one leg in one step walk. The step-length is a parameter value that can be adjusted and fixed in the control system. On the other hand, the foot-height is defined by applying ellipse formulation, like shown in gait trajectory pattern at Fig. 3. In case of walking forward and backward, the foot height at z-axis is defined in (30). Meanwhile during side steps, the foot height is defined in (31).

$$z = b \left( 1 - \frac{x^2}{a^2} \right)^{\frac{1}{2}} - h \quad (30)$$

$$z = b \left( 1 - \frac{y^2}{a^2} \right)^{\frac{1}{2}} - h \quad (31)$$

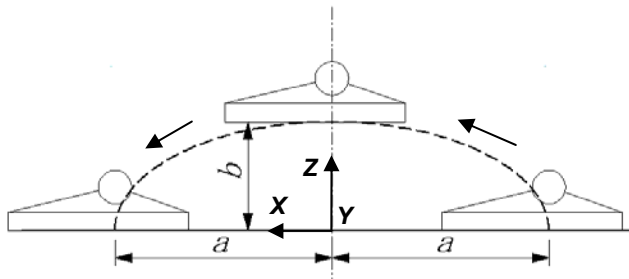


Fig. 3. Gait trajectory pattern of robot leg.

Here,  $h$  is hip-joint height from the ground. In real-time operation, biped locomotion is performed by giving the leg's end point position to the robot control system so that joint angle at each joint can be calculated by inverse kinematics formulations. Consequently the joint rotation speed and biped trajectory pattern are controlled by formulations of interpolation. By applying these formulations, each gait motion is performed in smooth and controlled trajectory.

#### 4. Analysis of Biped Trajectory Locomotion

It is inevitable that stable walking gait strategy is required to provide efficient and reliable locomotion for biped robots. In the biped locomotion towards application in unseen environment, we identified three basic motions: walk forward and backward directions, side-step to left and right, and yawing movement to change robot's orientation. In this section, we performed analysis to define efficient walking gait locomotion by improvement of walking speed and travel distance without reducing reduction-ratio at joint-motor system.

This is because sufficient reduction-ratio is required by the motor systems to supply high torque to the robot's manipulator during performing tasks such as object exploration and obstacle avoidance. We also present optimum yawing motion strategy for humanoid robot to change its orientation within confined space.

#### 4.1 Human Inspired Biped Walking Characteristics

Human locomotion stands out among other forms of biped locomotion chiefly in terms of the dynamic systems point of view. This is due to the fact that during a significant part of the human walking motion, the moving body is not in static equilibrium. The ability for humans to perform biped locomotion is greatly influenced by their learning ability (Dillmann, 2004, Salter et al., 2006). Apparently humans cannot walk when they are born but they can walk without thinking that they are walking as years pass by. However, robots are not good at learning. They are what they are programmed to do. In order to perform biped locomotion in robots, we must at first understand human's walking pattern and then develop theoretical strategy to perform the correct joint trajectories synthesis on the articulated chained manipulators at the robot's legs.

Figure 4 shows divisions of the gait cycle in human which focusing on right leg. Each gait cycle is divided into two periods, stance and swing. These often are called gait phase. Stance is the term used to designate the entire period during which the foot is on the ground. Both start and end of stance involve a period of bilateral foot contact with the floor (double stance), while the middle portion of stance has one foot contact. Stance begins with initial contact of heel strike, also known as initial double stance which begins the gait circle. It is the time both feet are on the floor after initial contact. The word swing applies to the time the foot is in the air for limb advancement. Swing begins as the foot is lifted from the floor. It was reported that the gross normal distribution of the floor contact periods is 60% for stance and 40% for swing (Perry, 1992). However, the precise duration of these gait cycle intervals varies with the person's walking velocity. The duration of both gait periods (stance and swing) shows an inverse relationship to walking speed. That is, both total stance and swing times are shortened as gait velocity increases. The change in stance and swing times becomes progressively greater as speed slows.

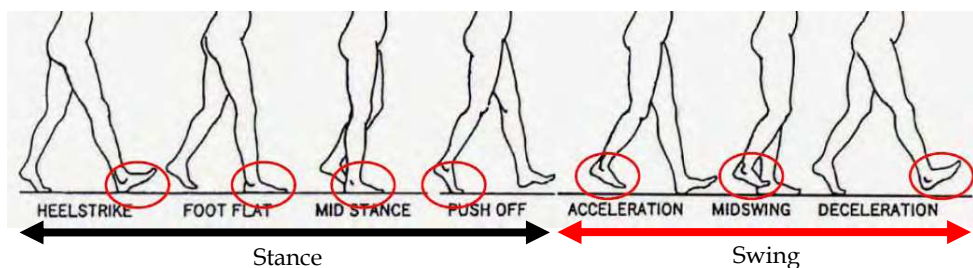


Fig. 4. Walking gait cycle in human.

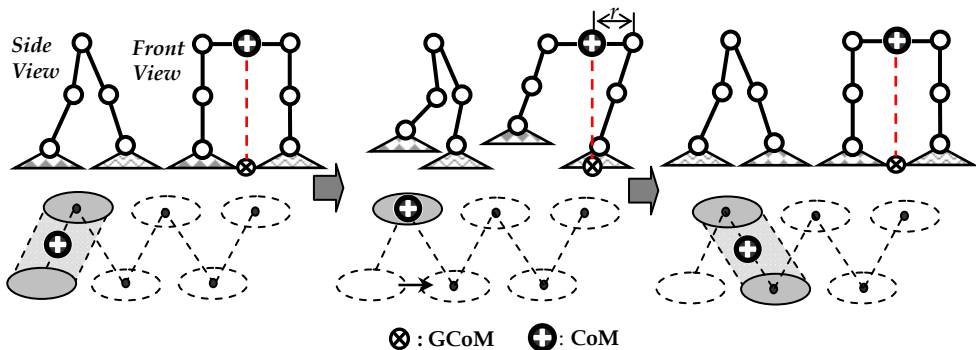


Fig. 5. Static walking model for biped robot in one cycle.

In contrast, for a biped robot two different situations arise in sequence during the walking motion: the statically stable double-support phase in which the whole structure of the robot is supported on both feet simultaneously, and the statically unstable single-support phase when only one foot is in contact with the ground, while the other foot is being transferred from back to front. Biped walking robot can be classified by its gait. There are two major research areas in biped walking robot: the static gait and dynamic gait. To describe gait motion in walking robots, it is easier to at first look at the static walking pattern point of view. In static walking pattern, two terms are normally used: Center of Mass (CoM) and Ground Projection of Center of Mass (GCoM). It is understood that to realize a stable gait motion, Center of Mass (CoM) and Ground Projection of Center of Mass (GCoM) must be in a straight line where the GCoM must always be within the foot sole area, as shown in Fig. 5. If GCoM is outside of the foot sole area, the robot will lose balance and fall down.

Notice that when swinging one leg, the waist moves to be on top of another leg in order to shift CoM position so that the CoM is centered with the GCoM. These movements bring together the whole robot trunk to left and right simultaneously. Therefore, to safely navigate the biped locomotion in a humanoid robot, it is necessary to consider the trunk movement of the robot body. In this study, the trunk movement is considered as a parameter value  $r$ , as shown in Fig. 5, which is taken as the distance from waist-joint to hip-joint. Eventually, this kind of walking pattern delays the walking speed. Moreover, joint structure design in robots does not permit flexible movement like that of human being. Indeed, one motor only can rotate in one direction. Even by reducing reduction-ratio can increase the motor rotation, it will eventually reduce the torque output which is not desirable for real-time operation.

Therefore, instead of stabilization issue that have been presented in many research, analysis to increase walking speed is necessary in biped locomotion so that the robots can move faster without reducing the reduction-ratio at the motor system, which will jeopardize their ability to perform tasks. Furthermore, not many works have been reported regarding analysis of biped walking speed.

#### 4.2 Analysis of Biped Walking Speed

We have identified that five main tasks need to be solved in the contact-based navigation system for biped robots: searching, self-localization, correction, obstacle avoidance, and object handling. On top of these tasks, walking locomotion is the basic motion that supports

the tasks. It is therefore an efficient biped locomotion strategy in walking motion is required in the navigation system. For the sake of navigating a biped humanoid robot, the objective is to generate efficient gait during performing tasks and maintain in stable condition until the tasks are completed.

The efficiency in biped robots is normally related with how fast and how easy the tasks can be completed. In fact, a method to control sufficient walking speed in conjunction with the biped gait trajectory is inevitably important. This is because in real-time application, the robots are likely to be required to walk faster or slower according to situation that occurred during the operation. It is therefore we need to identify parameters to control walking speed in biped locomotion. Previously, several studies have been reported related with walking speed of biped robot. For example Chevallereau & Aouste (Chevallereau & Aouste, 2001) have studied optimal reference trajectory for walking and running of a biped robot.

Furthermore, Yamaguchi (Yamaguchi et al., 1993) have been using the ZMP as a criterion to distinguish the stability of walking for a biped walking robot which has a trunk. The authors introduce a control method of dynamic biped walking for a biped walking robot to compensate for the three-axis (pitch, roll and yaw-axis) moment on an arbitrary planned ZMP by trunk motion. The authors developed a biped walking robot and performed a walking experiment with the robot using the control method. The result was a fast dynamic biped walking at the walking speed of 0.54 s/step with a 0.3 m step on a flat floor. This walking speed is about 50% faster than that with the robot which compensates for only the two-axis (pitch and roll-axis) moment by trunk motion. Meanwhile, control system that stabilizes running biped robot HRP-2LR has been proposed by Kajita (Kajita et al., 2005). The robot uses prescribed running pattern calculated by resolved momentum control, and a running controller stabilizes the system against disturbance.

In this research, we focus in developing efficient walking locomotion by improving the walking gait velocity and travel distance. This analysis employs the humanoid robot Bonten-Maru II as an analysis platform. Eventually, it is easy to control the walking speed by reducing or increasing the reduction-ratio at the robot joint-motor system. However, in real-time operation it is desirable to have a stable and high reduction-ratio value in order to provide high torque output to the robot's manipulator during performing tasks, such as during object manipulation, avoiding obstacle, etc. Therefore the reduction-ratio is required to remain always at fixed and high value.

#### 4.2.1 Selection of Parameters

The main consideration in navigating a biped humanoid robot is to generate the robot's efficient gait during performing tasks and maintain it in a stable condition until the tasks are completed. The efficiency in biped robots is normally related with how fast and how easy the tasks can be completed. In this research, to increase walking speed without changing the reduction-ratio, we considered three parameters to control the walking speed in biped robot locomotion:

- 1) Step length;  $s$
- 2) hip-joint height from the ground;  $h$
- 3) Duty-ratio;  $d$

Figure 6 shows initial orientation of Bonten-Maru II during motion mode which also indicate the step length and hip-joint height of the robot. The step-length is the distance between ankle-joints of a support leg and a swing leg when both of them are settled on the

ground during walking motion. The hip-joint height is the distance between intersection point of hip-joint roll and pitch to the ground in walking position. Meanwhile, duty-ratio for biped robot mechanism is described as time ratio of one foot touches the ground when another foot swing to transfer the leg in one cycle of walking motion.

In biped gait motion, two steps are equal to one cycle (refer Fig. 5). Figure 6 also shows link dimension of the Bonten-Maru II body and structure of the leg. The link parameters at the legs are used in calculations to define hip-joint height and maximum step length by geometrical analysis. Link parameters of the legs were calculated geometrically to define relation between step-length and hip-joint height. From the geometrical analysis, relation between the step-length and the hip-joint height is defined in Table 2.

At joint-motor system of Bonten-Maru II, maximum no-load rotation for the DC servomotor at each joint is 7220 [rpm]. This rotation is reduced by pulley and harmonic drive-reduction system to 1/333, in order to produce high torque output during performing tasks. We considered that the robot required high torque to perform tasks; therefore we do not change the reduction-ratio, which is 333:1. Eventually, these specifications produced maximum joint angular velocity at 130 [deg/s]. However, for safety reason, the joint angular velocity at the motor was reduced to 117 [deg/s].

The step time can be adjusted in the robot control system easily. However, if the step time is too small in order to increase walking speed, the robot motion becomes unstable. Moreover, the maximum step length performed becomes limited. In current condition, the step time for Bonten-Maru II to complete one cycle of walking is fixed between 7~10 second at maximum step length 75 [mm]. The duty-ratio  $d$  is increased gradually from 0.7 to 0.85.

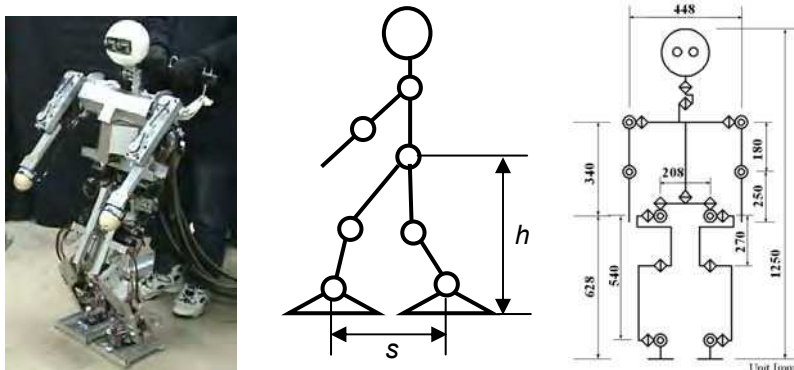


Fig. 6. Orientation of Bonten-Maru II to perform motion, parameters of hip-height  $h$  and step length  $s$ , and diagram of link dimensions.

Hip-joint height [mm]	Max. step length in 1 step [mm]	Max. step length in 1 cycle [mm]
$h_1=468$	350	700
$h_2=518$	300	600
$h_3=568$	200	400

Table 2. Relationship of step length against hip-joint height at Bonten-Maru II.

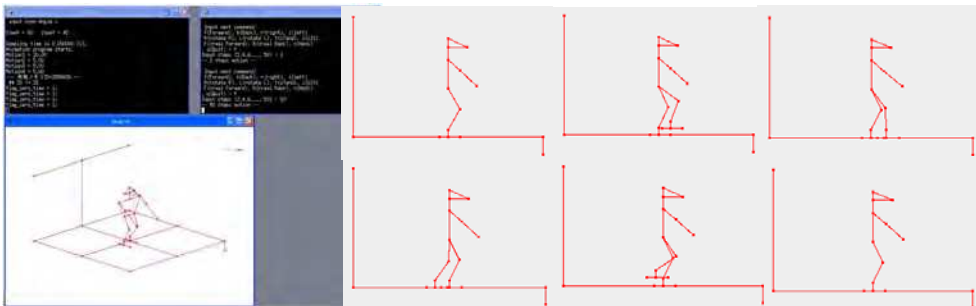


Fig. 7. Simulation by animation presents robot's trajectory in biped walking motion.

#### 4.2.2 Simulation Analysis

A simulation analysis of the robot walking velocity using animation that applies GnuPlot was performed based on parameters condition explained at previous section. The time for one circle of walking gait is initially fixed at 10 second. Figure 7 displays the animation screen of the robot's trajectory, which features a robot animation performing walking motion. Each joint's rotation angles are saved and analyzed in a graph structure. Based on the joint angle, angular velocity of each joint was calculated.

For example, Fig. 8 shows joint angle data for right leg joints when performing 10 steps walk at condition:  $h=518$  [mm],  $s=100$  [mm] and  $d=0.7$ . From the angle data, angular velocity for each joint was calculated and presented in Fig. 9. The first and last gait shows acceleration and deceleration of the gait velocity. The three steps in the middle show maximum angular velocity of the legs joint. Basically, in biped robot the maximum walking gait velocity is calculated from maximum joint angular velocity data by defining minimum step time for one gait. Eventually, by applying the same parameter, even if time for one step is initially different; the final joint angle obtained by the robot is same. Hence, in this analysis we can obtain the minimum step time in one step from the maximum joint angular velocity data that the initial step time was 10 seconds. Basically, the minimum gait time in one step is satisfying following equation:

$$t_{\min} < \frac{v_{\theta \max} \times 10}{V_{\theta \max}}. \quad (32)$$

Here,  $V_{\theta \max}$  is the maximum joint angular velocity at the motor,  $t_{\min}$  is minimum time for one step, and  $v_{\theta \max}$  is maximum joint angular velocity in each gait. Finally, the maximum walking gait velocity  $w_{\max}$  is defined by dividing length  $s$  with minimum step time  $t_{\min}$  in each gait, as shown in following equation.

$$w_{\min} = \frac{s}{t_{\min}} \quad (33)$$

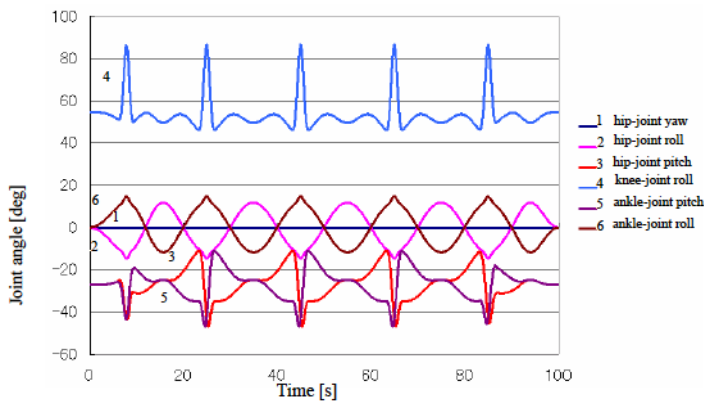


Fig. 8. Graph of joint rotation angle at right leg.

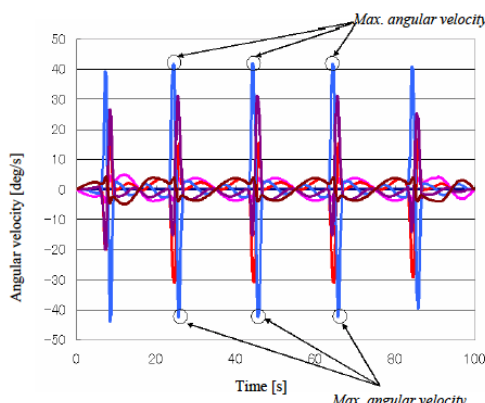


Fig. 9. Graph of angular velocity of joint rotation at right leg.

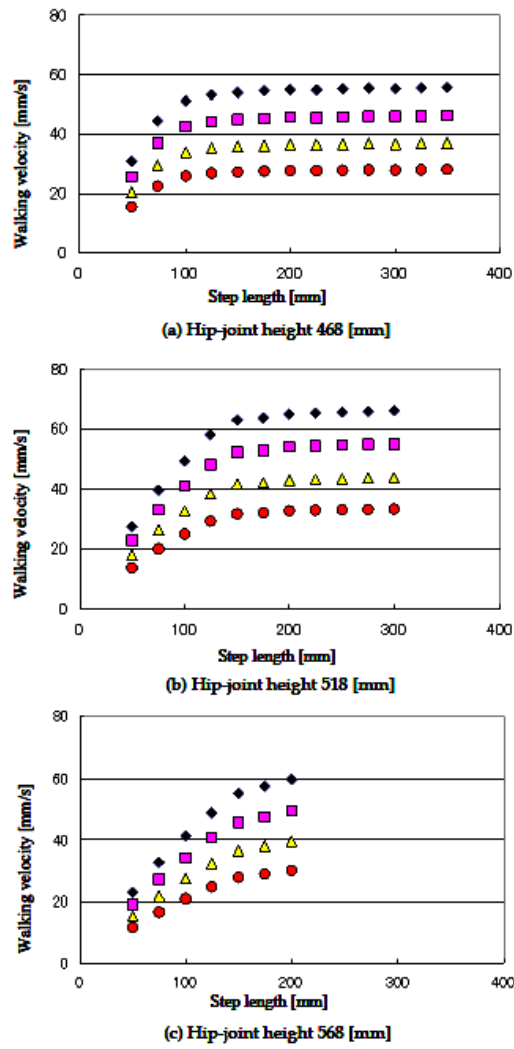


Fig. 10. Analysis results of maximum walking velocity at each gait.

#### 4.2.3 Simulation Results

Simulation results of walking gait velocity at each parameters value are compiled in graphs as shown in Fig. 10(a), (b) and (c). According to these graphs, from the relation of walking velocity and step length, the walking velocity was maintain nearly at constant value when it reached certain step length. Moreover, in relation of step length and hip-joint height, the higher hip-joint position is providing wider step length to perform better walking distance.

## Thank You for previewing this eBook

You can read the full version of this eBook in different formats:

- HTML (Free /Available to everyone)
- PDF / TXT (Available to V.I.P. members. Free Standard members can access up to 5 PDF/TXT eBooks per month each month)
- Epub & Mobipocket (Exclusive to V.I.P. members)

To download this full book, simply select the format you desire below

